

Dynamics of dilute and semidilute DNA solutions in the start-up of shear flow

Joe S. Hur and Eric S. G. Shaqfeh^{a)}

Department of Chemical Engineering, Stanford University, Stanford, California 94305

Hazen P. Babcock, Douglas E. Smith, and Steven Chu

Department of Physics and Applied Physics, Stanford University, Stanford, California 94305

(Received 13 June 2000; final revision received 31 October 2000)

Synopsis

We have investigated the dynamics of dilute ($10^{-5}C^*$) and semidilute ($\leq 6C^*$) DNA solutions both in steady and in the start-up of shear flow by combining fluorescence microscopy, bulk rheological measurements, and Brownian dynamics simulations. First, the microscopic states, i.e., the conformational dynamics of single DNA molecules in solution during the start-up of shear flow, were examined by fluorescence microscopy. To investigate the macroscopic response resulting from the changes in the microscopic state, the bulk shear viscosity of the same DNA solutions was also measured. While the transient dynamics of individual molecules is highly variable, an overshoot in the ensemble-averaged molecular extension is observed above a critical Wi following an overshoot in shear viscosity for both dilute and semidilute DNA solutions. These two overshoots are further analyzed and explained on a physical basis from our simulation findings. Based on the physical picture, we have derived a simple scaling to predict the strain at which an overshoot in shear viscosity occurs. Next, to study the effect of *intermolecular* interactions on the dynamics at steady state, the microscopic states of dilute and semidilute DNA solutions in steady shear flow were experimentally examined. We find that, for both the steady and the start-up of shear flow, when time is scaled with the longest polymer relaxation time, i.e., when we compare the chain dynamics at the same Wi , no measurable change in the character of the individual chain dynamics is observed in DNA solutions up to six times the overlap concentration (C^*). © 2001 The Society of Rheology. [DOI: 10.1122/1.1339246]

I. INTRODUCTION

Understanding the dynamics of a single polymer chain under various flow conditions has been a main focus in the development of constitutive models [Bird *et al.* (1987); Larson (1988); Doi and Edwards (1986)]. The assumption of “infinite dilution” or, equivalently, the neglect of intermolecular interactions is implicit in these studies. Until very recently, experimental measurements in solutions where the infinite dilution assumption could unambiguously be made were not possible. Thus, a direct comparison between various polymer models assuming infinite dilution and experimental results with finite polymer concentrations has been questionable. Moreover, the effect of concentra-

^{a)}Author to whom correspondence should be addressed; electronic mail: eric@chemeng.stanford.edu

tion on the dynamic properties of polymer solutions has been observed in some light-scattering measurements and birefringence studies even for very small concentrations [Ng and Leal (1993); Link and Springer (1993); Evans *et al.* (1994); Lee *et al.* (1997)].

With the advancement of experimental techniques such as single-molecule fluorescence microscopy, recent years have seen much progress in investigating the dynamics of single polymers, in particular DNA molecules, in various flows which has helped us gain insight into the microscopic behavior of polymers [Perkins *et al.* (1994); Perkins *et al.* (1995); Perkins *et al.* (1997); Smith and Chu (1998); Smith *et al.* (1999); Doyle *et al.* (2000)]. Furthermore, numerical simulations and theories have provided us with useful information to deepen our understanding of many interesting experimental observations [Larson *et al.* (1997); Cifre and de la Torre (1999); Larson *et al.* (1999); Lyulin *et al.* (1999); Li and Larson (2000); Dua and Cherayil (2000); Doyle *et al.* (2000), Hur *et al.* (2000)].

In this work, we have investigated the transient dynamics of polymer molecules subject to the inception of shear flow in solutions of varying polymer concentration. The main experimental findings, as well as some preliminary analysis of our experimental results, have been recently reported in a separate article [Babcock *et al.* (2000)]. We note that in this paper, we have extended our analysis such that it is more quantitative and we have also included other important experimental results, as well as simulation findings that were not included in our previous publication due to space limitations.

In addition to well-known rheological behavior such as shear thinning in steady shear flow, polymer solutions often demonstrate interesting transient behavior in the start-up of shear flow. For example, an overshoot in a number of macroscopic rheological properties, including the shear viscosity, the first normal stress, and the birefringence, have been widely observed to occur above a critical shear rate for dilute and concentrated solutions [Huppler *et al.* (1967); Chow *et al.* (1985); Magda *et al.* (1993); Kume *et al.* (1997); McLeish *et al.* (1999)]. The qualitative aspects of these experimental findings have been predicted by various simulations and theories [Liu (1989a, 1989b); van den Brule (1993); Öttinger (1995); Carl (1997); Doyle and Shaqfeh (1998)]. However, to date a clear physical understanding of how overshoots in the various macroscopic properties are related both to each other and to the changes in the microscopic states of the polymer molecule is not well established.

To investigate the transient dynamics of polymer solutions, we have used the λ -DNA molecule as our model polymer. We have combined single-molecule fluorescence microscopy, bulk rheological measurements, and Brownian dynamics simulations to gain insight into the nature of the overshoot in the rheological properties. Such an approach has been proven effective in our previous work [Smith *et al.* (1999); Hur *et al.* (2000)]. To examine the effect of concentration, i.e., chain interactions on the dynamics, we have also studied DNA solutions with varying concentrations from $10^{-5}C^*$ ($C^* \equiv$ overlap concentration) up to $6C^*$ in both steady and the start-up of shear flow.

This paper is organized as follows. In Sec. II A we discuss sample preparation as well as our experimental methods including fluorescence microscopy. A brief description of the shear apparatus is given. By analyzing the chain retraction from an extended state, we extract the molecular time scale (λ) necessary to characterize the flow strength as presented in Sec. II A 3. In Secs. II A 4 and II A 5 experimental findings showing an overshoot in molecular extension at a high Weissenberg number (Wi) for DNA in both dilute and semidilute solution are presented. The Weissenberg number is defined as the shear rate $\dot{\gamma}$ times the relaxation time of the polymer chain λ . The probability distribution function (PDF) of molecular extension as a function of the shear strain ($\dot{\gamma}t$) is also analyzed at low and high values of Wi for both types of solutions. To examine the

temporal fluctuations of the molecules at steady state, the power spectral density (PSD) of the molecular extension in solutions at various concentrations is analyzed in Sec. II A 6, as previously reported [Smith *et al.* (1999); Hur *et al.* (2000)]. In Sec. II B 1, the macroscopic rheological properties of $1C^*$, $3C^*$, and $6C^*$ DNA solutions in both steady and the start-up of shear flow are characterized. Finally, to connect the microscopic and macroscopic observations in experiment, we use Brownian dynamics simulation of Kramers' freely jointed chains matching the number of Kuhn steps of the λ -DNA molecules used in the experiment. In Sec. III A a brief description of our model and simulation method is presented. We directly compare our simulation results to the observed overshoots in molecular extension and polymer shear viscosity in Secs. III B and III C. Our analysis of these results allows us to answer the question we have initially posed—namely, how are macroscopic properties of polymer solutions in the start-up of a shear flow associated with the changes in the microscopic states of the molecules in solution? In Sec. IV we summarize our main findings with a brief conclusion.

II. EXPERIMENT

A. Single-molecule fluorescence microscopy

1. Sample preparation

Fluorescently labeled bacteriophage lambda DNA (λ -DNA) was prepared using the following protocol. A solution of 10^{-5} M YOYO-1 (Molecular Probes, Eugene, OR) was made by diluting stock YOYO-1 solution (10^{-3} M) by a factor of 100 in TE10 buffer (10 mM tris-HCl, 1 mM EDTA, 10 mM NaCl, pH 8). Then, stock λ -DNA (Gibco BRL, Gaithersburg, MD) at a concentration of ~ 0.5 mg/ml was diluted by a factor of 50 in TE10 and heated to 65 °C for 10 min to free the DNA's complementary sticky ends. After the DNA solution had cooled to room temperature, the DNA solution was diluted by a factor of 40 into a solution that was made by mixing 100 parts TE10 and 1 part 10^{-5} M YOYO-1 solution. The DNA/dye solution was then allowed to sit for at least 1 h at room temperature in the dark before being used. λ -DNA stained in this fashion was previously found to have a contour length of approximately 21–22 μm [Perkins *et al.* (1995)]. To the best of our knowledge, the Kuhn length of stained λ -DNA molecules has not been measured thoroughly. Thus, in our previous work [Hur *et al.* (2000)], to account for the ambiguity of the exact number of Kuhn steps, we have varied the number of rods (a rod being equivalent to a Kuhn step for Kramers' chains) in the simulations. We found that the dynamics of a Kramers' chain consisting of 220 Kuhn steps is both qualitatively and quantitatively similar to that of a chain consisting of 150 Kuhn steps in steady shear flow. We also note that there is an uncertainty as to the exact contour length of a fluorescently labeled λ -DNA molecule, and depending on the amount of the dye used, it is known to be between 18 and 22 μm [Perkins *et al.* (1997); Smith and Chu (1998); Smith *et al.* (1999); Doyle *et al.* (2000)]. In this work, we have used a value of 22 μm for the contour length to normalize the experimental data. For reference, unstained λ -DNA has a hydrodynamic radius of 2 nm [Pecora (1991)] and a persistence length of 53 nm and a total length of 16.3 μm [Bustamante *et al.* (1994)].

The 60 and 220 cP buffers were of the following composition, $\sim 55\%$ (w/w) sucrose (220 cP) or $\sim 40\%$ (w/w) sucrose (60 cP), 18% (w/w) glucose, 4% β -mercaptoethanol, 10 mM tris-HCl (pH 8.5), 2 mM EDTA, and 10 mM NaCl. A viscometer was used to measure the solution viscosities, and they were adjusted if necessary by varying the sucrose concentration. These buffers were used for measurements at a concentration of $10^{-5}C^*$ and $Wi = 6.3(60\text{ cP}), 13(60\text{ cP}), 19(220\text{ cP}),$ and 38 (220 cP). As is usually done [Doi and Edwards (1986); Larson (1988)], we define C^* as the concentration at

which a random equilibrium coil of radius R_g would begin to overlap with nearby coils ($C^* = (M_w/N_A 4/3) \pi R_g^3$), where M_w is the molecular weight and N_A denotes the Avogadro's number. For our λ -DNA solutions C^* is about 0.04 mg/ml based on a measured radius of gyration of 0.7 μm for the unstained DNA. Buffers that were used for the remaining measurements in solutions of 10^{-5} , 0.5, 1.0, and $6.0C^*$ were made as follows. First, a solution of 10 mM tris-HCl (pH 8.5), 1 mM EDTA, 10 mM NaCl, 10% (w/w) glucose, and approximately 65% (w/w) sucrose was made. The sucrose concentration was adjusted such that when 89 parts of the buffer solution was mixed with 11 parts of water, the resulting solution had a viscosity of 100 cP. The solutions with $10^{-5}C^*$ background polymer concentration used for the $Wi = 16$ and 48 data sets were made by mixing 890 μl of the buffer stock with 80 μl of distilled water. 890 μl of the buffer stock was mixed with 40 μl of distilled water and 40 μl of stock λ -DNA to make the $0.5C^*$ solutions. $1.0C^*$ solutions were composed of a mixture of 890 μl of buffer and 80 μl of λ -DNA. Finally, to make $6.0C^*$ solutions, 3.85 g of sucrose and 0.6 g of glucose were dissolved in 2.4 ml of stock λ -DNA solution that had been heated to 65 $^\circ\text{C}$ for 10 min and cooled to room temperature. The resulting solution, if made with water rather than stock λ -DNA solution, had a viscosity of 100 cP when 1 ml was mixed with 30 μl of water.

For experiments with 60 and 220 cP buffers, 1 ml of the appropriate buffer was mixed with 10 μl of a solution (GLOX) containing glucose oxidase (5 mg/ml) and catalase (1 mg/ml) in TE10. When the 100 cP buffer was used, 10 μl of GLOX solution and 10 μl of β -mercaptoethanol were mixed with 870 ml of buffer with the appropriate background polymer concentration (10^{-5} , 0.5, or $1.0C^*$). $6.0C^*$ samples were prepared by adding 10 μl of GLOX and 10 μl of β -mercaptoethanol to 1 ml of $6.0C^*$ polymer solution. Then, for all samples, 10 μl of a 1:2 dilution of the fluorescently labeled λ -DNA solution was added and the entire sample was pipetted into the shear apparatus. To minimize evaporation, samples in the apparatus were covered with 1 ml of mineral oil.

2. Experimental procedures

The shear apparatus created a uniform simple shear flow by the translation of two parallel glass plates separated by $\sim 50 \mu\text{m}$ past one another, as shown in Fig. 1 [Smith *et al.* (1999)]. The bottom plate was a 1.5 cm \times 5.7 cm No. 2 glass coverslip through which fluorescently labeled λ -DNA could be visualized. It was glued onto the bottom of a 3.7 cm \times 0.9 cm channel milled into a piece of acrylic plastic. A wafer saw was used to cut a piece of glass 1.9 cm \times 0.3 cm from a microscope slide. This piece of glass, which acted as the top plate in the shear cell, was then glued onto a rigid support. The support was held against three micrometer screws by two stiff springs, allowing one to level the upper plate relative to the lower plate and to adjust the size of the gap between them with less than 5% variation. This assembly was mounted onto a translation stage (No. 426, Newport, Irvine, CA), which was driven by an optically encoded dc motor (Oriental Motor, Stratford, CT) with $\sim 2\%$ root-mean-square speed variation. The translation stage was mounted onto an aluminum plate whose angle relative to the bottom surface of the shear cell could be adjusted by a micrometer screw. This was done so that the translation stage could be made level to the bottom surface of the shear cell, which would keep the size of the gap constant as the surfaces were translated past each other. The shear apparatus was placed onto the stage of a homebuilt inverted microscope equipped for epifluorescence. A 100 W mercury arc lamp (Zeiss, Thornwood, NY) was used as an excitation source. Light from the lamp was passed through a $470 \pm 20 \text{ nm}$ bandpass excitation filter (Omega, Brattleboro, VT). Then, it was reflected by a 500 mm long-pass dichroic (Chroma,

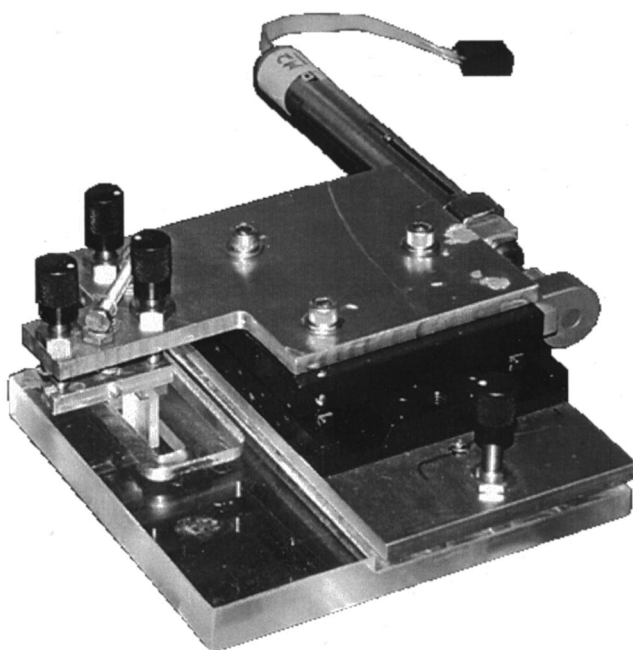


FIG. 1. Shear apparatus used for single-molecule microscopy.

Brattleboro, VT) into the back of a $60\times$, 1.2 numerical aperture water immersion objective (Nikon). A 160 mm to infinity correction collar (Zeiss) was used to correct the objective. The objective focused the excitation light onto the sample and also collected the fluorescence emission from the dye. The collected light passed through the dichroic and a 515 nm long-pass emission filter (Omega). A 40 cm tube lens focused the collected light onto a microchannel-plate image intensifier (Hamamatsu) that was coupled by a fiber taper to a video camera [charge-coupled device (CCD) Phillips]. The camera imaged a $90\ \mu\text{m}\times 65\ \mu\text{m}$ area in the focal plane of the microscope. The output of the video camera was either two- or four-frame averaged with an image processor (Hamamatsu) and captured directly to the hard disk of a computer using an image capture board (National Instruments) and custom software. To follow the dynamics of a polymer in the start-up of shear flow, a coiled molecule at equilibrium was first positioned at one end of the imaging area. Then, the motor that translated the entire shear apparatus relative to the imaging optics was started. When the molecule reached the center of the imaging area, the motor that translates the top plate relative to the bottom plate was started. This produces a start-up shear flow, and if the correct velocities were chosen for the motors, the molecule would remain in the imaging area. As the data run progressed, the speed of the motor that moved the apparatus relative to the optics had to be adjusted to keep the molecule in the field of view. The extension of the molecule in the shear flow direction projected in the flow-vorticity plane was measured directly from the captured video images.

3. Chain relaxation

The dimensionless number characterizing the ratio between the Brownian forces (or, equivalently, the thermal fluctuations due to the surrounding medium) and the imposed flow strength is the Weissenberg number, Wi . The Wi is thus simply the ratio of the chain

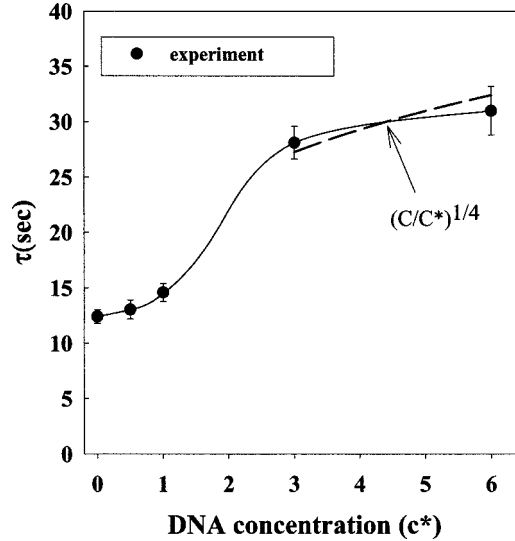


FIG. 2. Longest polymer relaxation time (τ) of 10^{-5} , 0.5, 1.0, 3.0, and $6.0C^*$ DNA solutions. The solid line is to guide the eye. For comparison, we show the predicted scaling of the longest relaxation time of semidilute polymer solutions by de Gennes (1979) for DNA concentrations higher than $3C^*$ (the dashed line).

diffusion time scale (t^D) (to characterize Brownian motion-induced configuration changes) to the characteristic flow time scale ($1/\dot{\gamma}$). A relevant, and also a widely used diffusion time scale for a polymer chain, is the longest polymer relaxation time (λ) which, for example, depends on the surrounding medium and the temperature. In order to measure λ we maintained the solvent viscosity at 90–100 cP and made the measurements for a variety of DNA concentrations. DNA molecules were first stretched to $\sim 50\%$ of the contour length in shear flow. The flow was then stopped and the images of the DNA molecules were recorded and analyzed, as outlined in Sec. II A 2.

The chain retraction can be related to the decay in normal stress (τ_{11}), by which the bulk relaxation time of a polymer solution is usually measured [Bird *et al.* (1987)], as follows. When the chain is stretched $< 30\%$ – 40% of its contour length [Bird *et al.* (1987)],

$$\tau_{11} = n_p \langle R_1 F_1^c \rangle \approx n_p H \langle R_1 R_1 \rangle, \quad (1)$$

where R_1 is the end-to-end distance of the molecule in direction “1” along which the molecule is initially extended. F^c is the entropic force of the molecule, n_p is the number density, H is a spring constant, and the brackets denote an averaged quantity. This shows that the longest relaxation time obtained from measuring the normal stress decay upon flow cessation can be directly related to that from measuring the chain retraction.

By fitting the chain retraction to a single-exponential decay function,

$$\langle R_1 R_1 \rangle = A \exp\left(-\frac{t}{\lambda}\right) + B, \quad (2)$$

we can calculate λ . In Eq. (2) A and B are fitting parameters. In Fig. 2 we show the longest polymer relaxation time of DNA solutions with varying concentrations obtained from an ensemble of 50–60 molecules for each concentration. Note that our measured

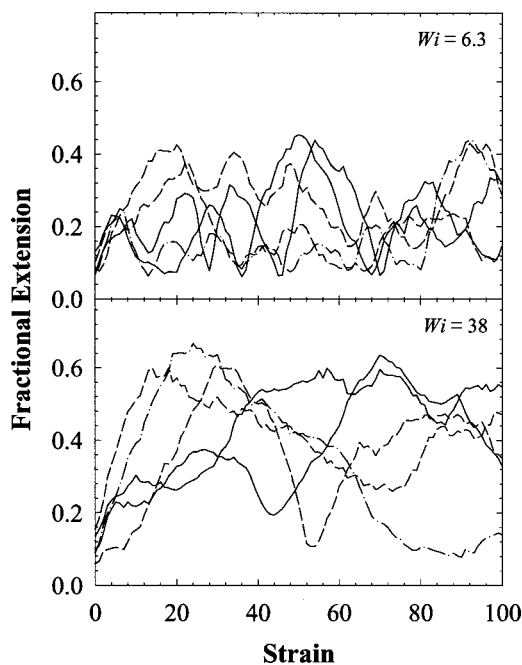


FIG. 3. Fractional molecular extension of five different DNA molecules on flow inception shows molecular individualism. The variance increases with Wi .

relaxation time is consistent with that predicted by de Gennes (1979) at DNA concentrations higher than $3C^*$, where the relaxation time of semidilute polymer solutions was shown to scale as

$$\lambda \sim \left(\frac{c}{c^*} \right)^{1/4}. \quad (3)$$

4. Transient shear dynamics: Dilute solution

As shown in Fig. 3, DNA molecules take widely different paths at the start-up of shear flow. This molecular individualism has also been observed in elongational flow [de Gennes (1997); Perkins *et al.* (1997); Smith and Chu (1998); Larson *et al.* (1999)]. The difference in the transient behavior of DNA molecules can be attributed in part to the wide spectrum of equilibrium configurations of each molecule upon flow inception [Perkins *et al.* (1997); Smith and Chu (1998)]. The fluctuations in molecular extension are shown to increase with Wi , implying that DNA molecules undergo more dramatic conformational changes at higher Wi even in the transient stage.

By averaging the molecular extension of an ensemble of DNA molecules, we can examine the “average” chain deformation. We have reported previously [Babcock *et al.* (2000)] that an overshoot in molecular extension is seen above $Wi = 19$. To briefly summarize the previous findings in Babcock *et al.* (2000), we observe an initial linear growth in the average molecular extension up to $\dot{\gamma}t = 5$ at all Wi (6, 13, 19, and 38) we studied. Interestingly, all initial stretch rates are shown to be independent of the Wi up to $Wi = 38$. A detailed discussion of the initial deformation is presented later in Sec. III B, where we compare the experimental results to our simulation findings. After the initial stretch, the average molecular extension tends to reach a plateau value with moderate

fluctuations for $Wi < 20$. The fluctuations about the mean value are due to the relatively small ensemble size (< 200) used in the experiments. We anticipate that the uncorrelated noise would be fully dampened if a larger ensemble were used. Above $Wi = 20$, a mild overshoot in average molecular extension is observed at $\dot{\gamma}t = 20\text{--}30$.

To investigate the overshoot, we have calculated the transient probability distribution function of molecular extension by binning the extension data at $Wi = 6$ and 38 , as shown in Fig. 4. At both values of Wi the initial PDF is Gaussian. At $Wi = 6$, where no overshoot in molecular extension was observed, the PDF broadens slowly with strain ($\dot{\gamma}t$), and at $\dot{\gamma}t = 40$ it has already reached its steady-state distribution, which takes the form of the skewed Gaussian with a peak at $L/D^{\max} = 0.2$. For $Wi = 38$, where a mild overshoot was observed, the distribution of molecular extension broadens more rapidly than that at $Wi = 6$. More interestingly, we observe a skewed distribution of extension larger than $L/L^{\max} = 0.6$ at $\dot{\gamma}t = 30$, which corresponds to the strain at which an overshoot is seen. At later strain, this skewed distribution is shifted to lower values of extension, and at $\dot{\gamma}t = 40$ we see an almost uniform broad distribution of chain extension as we have reported previously [Smith *et al.* (1999); Hur *et al.* (2000)]. This shift of higher molecular extension to smaller extension observed only at large values of Wi indicates that there is an average chain retraction above a critical value of Wi . We have reported previously that the overshoot of molecular extension is associated with the initial alignment of the chain in the flow [Babcock *et al.* (2000)] by verifying that no overshoot is observed when we calculate the evolution of the average molecular extension of transiently coiled molecules in steady state, i.e., by resetting the strain ($\dot{\gamma}t > 50$) where the molecule has retracted to a coil to $\dot{\gamma}t = 0$.

5. Transient shear dynamics: Semidilute solution

The study of dilute DNA solutions ($< 10^{-5}C^*$) in Sec. II A 4 has shown that an overshoot in average molecular extension occurs above a critical value of Wi . It is evident that this behavior is solely due to intramolecular interactions and solvent–polymer interactions since the dynamics of a single chain are not affected by surrounding chains for concentration, $C < 10^{-5}C^*$. To examine the effect of *intermolecular* chain interactions on the transient dynamics, we have used three DNA solutions of 0.5 , 1.0 , and $6.0C^*$ concentrations. These solutions lie near or in the so-called semidilute regime [Doi and Edwards (1986)] where individual chains are hypothetically in contact with one another at equilibrium.

One interesting question is how the presence of surrounding chains affects the dynamics of any given chain. We have reported an increase in chain relaxation time with increasing DNA concentration in Sec. II A 3. Thus, as a first approximation one might think of the surrounding chains as an effective viscous medium. If this was a complete model, then one must show that the dynamics of individual DNA molecules in solutions at varying polymer concentrations are equivalent when the time is scaled with the longest polymer relaxation time, i.e., when we compare the dynamics of DNA in solutions at different polymer concentrations but at the same values of Wi .

In Fig. 5, we show the molecular extension of 10^{-5} , 0.5 , 1.0 , and $6.0C^*$ solutions at values of $Wi = 45\text{--}60$. In a previous study, we have reported the evolution of molecular extension at lower values of Wi ($Wi = 19\text{--}41$) of these solutions [Babcock *et al.* (2000)]. Note that the Wi range is above the critical $Wi_c \approx 20$, where an overshoot in molecular extension was seen in *dilute* DNA solutions. Again, we see a mild overshoot in the molecular extension at $\dot{\gamma}t = 20\text{--}40$ in both cases. The initial deformation rate, as well as the overall shape of the average chain deformation upon flow inception, is similar

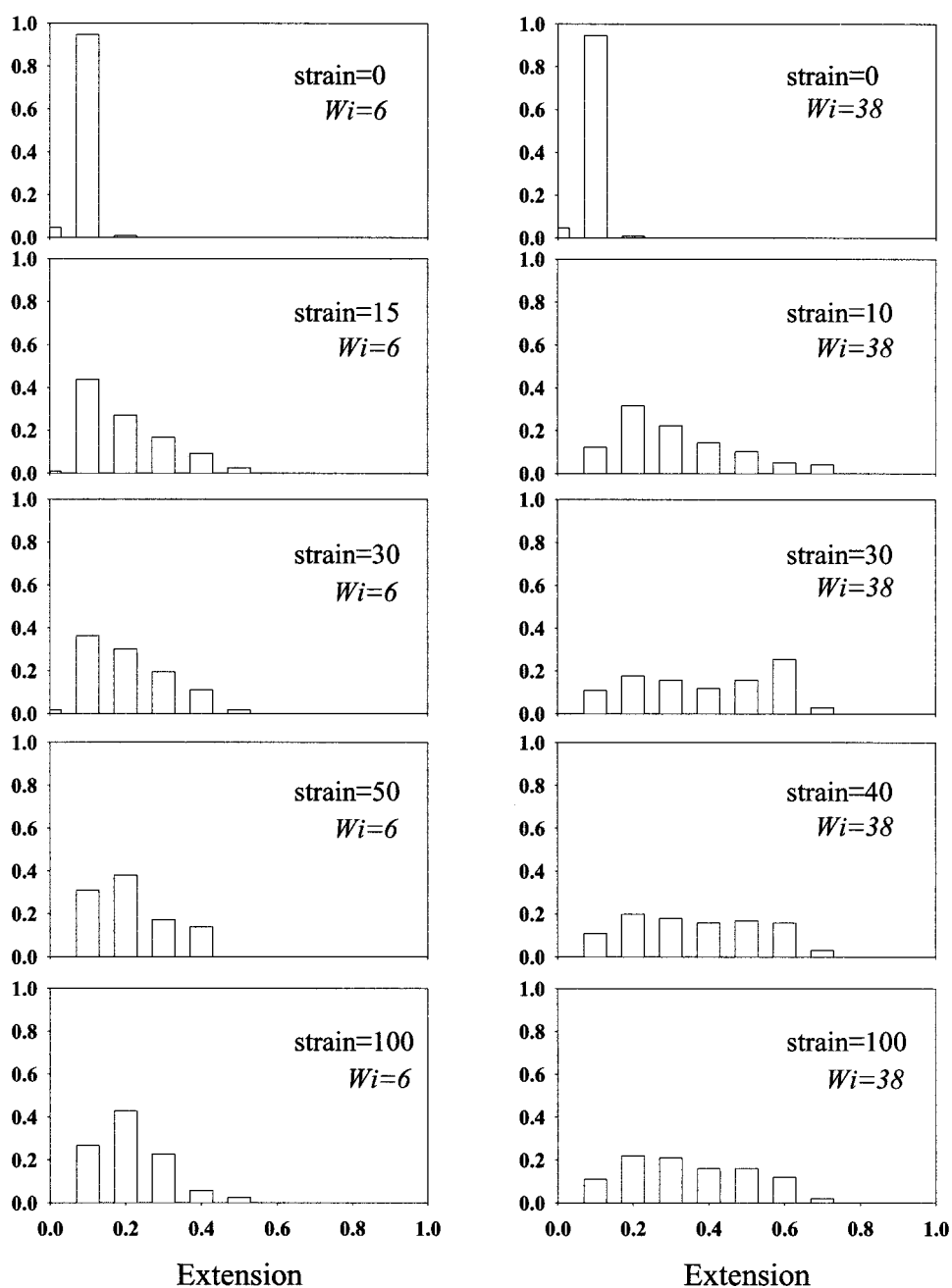


FIG. 4. Probability distribution function of molecular extension at $Wi = 6$ and 38. The molecular extension has been normalized with its contour length.

in character for all DNA solutions at comparable values of Wi . The transient PDF of molecular extension for a $1.0C^*$ DNA solution at $Wi = 19$ and 60 is shown in Fig. 6. Again, as in the case of our dilute DNA solutions, at the lower value of $Wi = 19$, the PDF broadens steadily and at $\dot{\gamma}t = 30$ it has reached its steady distribution. At $Wi = 60$, where an overshoot in molecular extension is seen, the PDF broadens and at $\dot{\gamma}t$

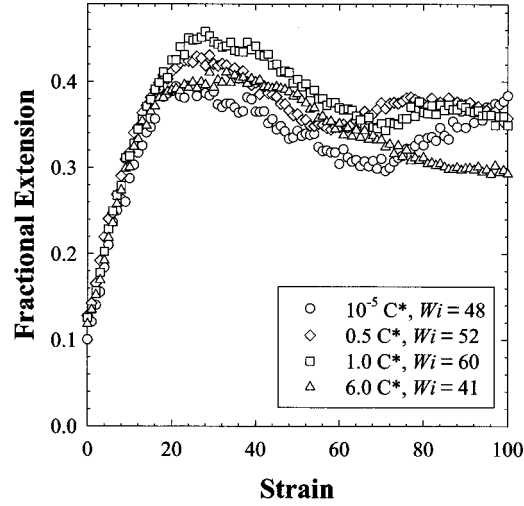


FIG. 5. Average molecular extension of DNA chains in semidilute solutions (10^{-5} , 0.5, 1.0, and $6.0C^*$) at near $Wi = 45$. All DNA solutions show an overshoot in molecular extension at $\dot{\gamma}t = 20$ –40.

$= 30$ we see a broad distribution of molecular extension (L/L^{\max}) with a maximum at $L/L^{\max} > 0.6$. The probability distribution of molecules extended more than 60% of its contour length ($L/L^{\max} > 0.6$) is almost as large as that of moderately extended ones ($0.2 < L/L^{\max} < 0.6$). However, at later strain the more extended molecules ($L/L^{\max} > 0.6$) are not seen in the PDF at $\dot{\gamma}t = 75$ and the configuration population is shifted towards smaller molecular extension. We note that this transient shift of more-extended molecules to a less-extended state at high Wi is also observed for 0.5 and $6.0C^*$ DNA solutions.

6. Steady shear dynamics: Dilute and semidilute solution

In previous sections, we have investigated the transient microscopic response of DNA solutions of varying concentrations. Note that the highest DNA concentration of $6.0C^*$ in this study is about a factor 2 less than the concentration ($\sim 13C^*$) where reptative behavior of DNA molecules was observed as reported previously [Perkins *et al.* (1994)]. The findings we have gathered from examining the microstates of DNA molecules in the start-up of shear flow suggest that the transient dynamics of semidilute DNA solutions can be understood by a simple model where an isolated single DNA molecule is placed in a more viscous medium to compensate for the increase in viscosity due to the surrounding chains. To further investigate this rather interesting observation we have looked into the dynamics of DNA solutions at various concentrations in *steady* shear flow.

Due to the fact that there is no single stable molecular configuration in steady shear flow [Smith *et al.* (1999); Hur *et al.* (2000)], DNA molecules tumble, stretch, and retract in a stochastic manner. One effective way of characterizing these fluctuations in the time domain is by taking the fast Fourier transform (FFT) of the autocorrelation of the fluctuating quantity, i.e., the chain extension in our case, and thus examining the frequency characteristics in the Fourier space. Our previous work showed that the power spectral density of molecular extension in steady shear flow has three distinct frequency regimes at finite Wi arising from the coupling of the hydrodynamic drag forces and the Brownian forces [Hur *et al.* (2000)].

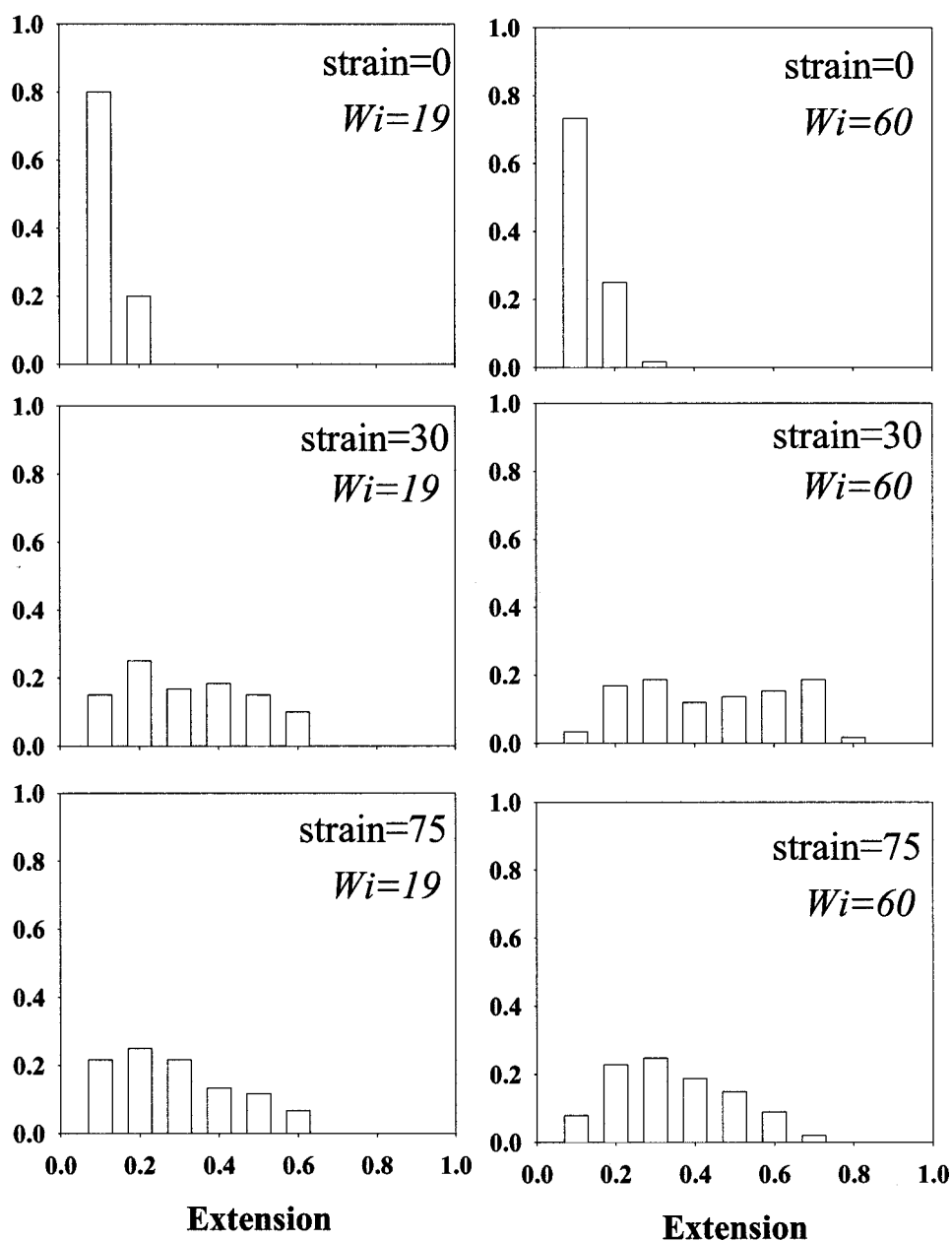


FIG. 6. Transient probability distribution function of molecular extension at $Wi = 19$ and 60 for $1.0C^*$. The molecular extension has been normalized by its contour length.

For consistency, we follow the same data analysis procedure for all our experimental data as well as the simulation data. We first subtract the mean value of the molecular extension at each Wi from the extension of a polymer chain and multiply by a Welch window [Hur *et al.* (2000)]. We then take the fast Fourier transform of this preprocessed data. To obtain the PSD, the resulting data from the FFT are further divided by the total sampling time in the simulation and then normalized according to Parseval's theorem. The maximum frequency is determined by the Nyquist frequency $f^{\max} = 1/2\Delta t$, where

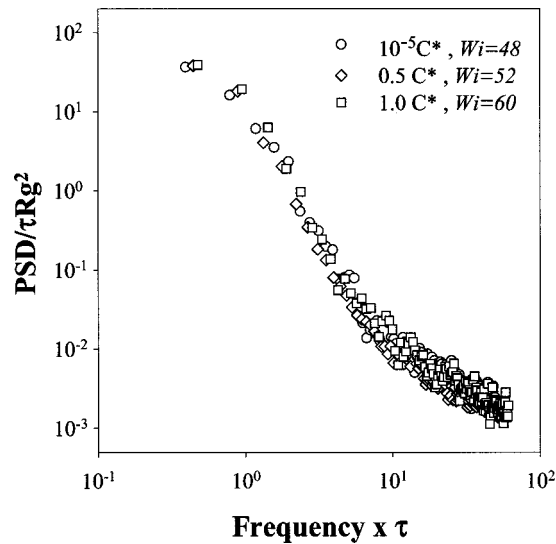


FIG. 7. Power spectral density of molecular extension at $Wi = 48$ – 60 for 10^{-5} , 0.5 , and $1.0C^*$ DNA solutions.

Δt is the time step in the simulation. Finally, the PSD is nondimensionalized by the square of the radius of gyration (R_g^2) and the longest relaxation time (λ). The frequency is made dimensionless with the longest relaxation time.

In Fig. 7, three distinct frequency regimes are demonstrated—a plateau regime at low frequency, followed by a pronounced decaying regime at intermediate frequency, and finally, a more slowly decaying regime at high frequency. The three different DNA solutions of 10^{-5} , 0.5 , and $1.0C^*$ concentrations show essentially no qualitative or quantitative difference at comparable values of Wi , confirming the fact that surrounding chains do not affect the steady dynamics of a given chain other than merely increasing the medium viscosity. We note that an overlap of the PSDs of these DNA solutions at lower values of Wi (17 – 20) has been reported in our previous article [Babcock *et al.* (2000)]. It is even more striking that the power spectra of a DNA molecule at concentrations of 10^{-5} and $6.0C^*$ DNA solutions at $Wi = 38$ – 41 , as shown in Fig. 8, demonstrate a perfect overlap, which again supports the aforementioned argument.

The steady-state PDFs of molecular extension at $Wi = 16$ – 19 and $Wi = 48$ – 60 in Fig. 9 show no qualitative and very little quantitative difference in chain population. All the PDFs have a broad spectrum of chain extension with the ones at high values of Wi showing a more uniform distribution. Finally, when we compare the steady average molecular extension in Fig. 10, within experimental error the normalized molecular extension monotonically reaches an asymptotic value of 0.4 for all DNA solutions. However, we point out that at the highest of concentration of $6.0C^*$, the value of average extension is lower by 15% – 25% than that of DNA solutions of lower concentration. The existence of such a low asymptotic value of 0.4 also seen at a DNA concentration of $10^{-5}C^*$ has been attributed in our previous work [Hur *et al.* (2000)] to a relatively large Graetz–Leveque layer in configuration space where the chain exists and, furthermore, the layer thickness was shown to depend very weakly on Wi [Hur *et al.* (2000)]. In this layer, a DNA molecule undergoes tumbling, stretching, and recoiling due to the coupling between the Brownian fluctuations along the gradient direction and the shear convection driving extension fluctuations [Hur *et al.* (2000)].

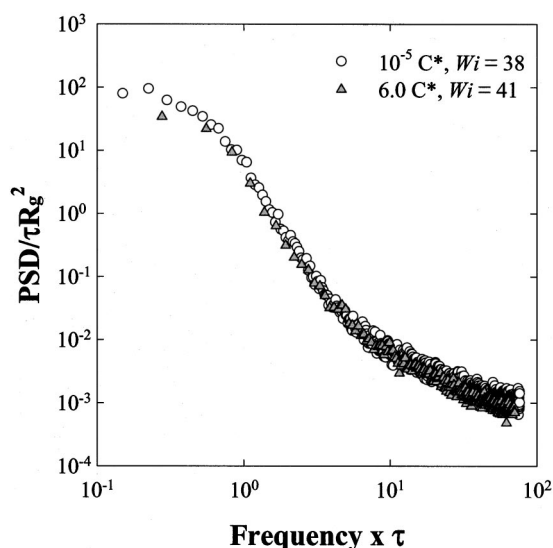


FIG. 8. Power spectral density of molecular extension at $Wi = 38$ – 41 for 10^{-5} and $6.0C^*$ DNA solutions.

The steady shear results presented in this section are consistent with our transient experimental findings showing no significant qualitative or quantitative difference (except perhaps small differences for the $6.0C^*$ solution) when the dynamics of DNA solutions of different concentrations are compared at the same or comparable values of Wi .

B. Rheological measurements

To establish a connection between the single-molecule microscopy experiments where the microscopic states of the DNA molecules were examined, the macroscopic rheological properties of the same DNA solutions were measured. The solutions were prepared following the same procedure as outlined in Sec. II A except that the small fractions ($< 10^{-5}C^*$) of fluorescently labeled DNA molecules were not added. All the rheological measurements were done at $21 \pm 0.5^\circ\text{C}$ using a shear viscometer (rheometric dynamic analyzer RDA II, RSI Scientific, Piscataway, NJ).

1. Steady shear rheology

To first characterize the DNA solutions the steady shear viscosities of the 1, 3, and $6C^*$ solution were measured. In Fig. 11 the polymer contribution to the steady shear viscosity is shown for solutions at three different concentrations. All the polymer shear viscosity data show shear thinning with a $Wi^{-\alpha}$ dependence where α is the shear-thinning exponent. We note that previous work has shown that the thinning exponent α for the steady polymer shear viscosity (η_{polymer}^s) in the case of the Kramers' chain with a large number of Kuhn steps ($N > 20$) is [Liu (1989a, 1989b); Doyle *et al.* (1997); Hur *et al.* (2000)]

$$\eta_{\text{polymer}}^s \sim Wi^{-1/2}. \quad (4)$$

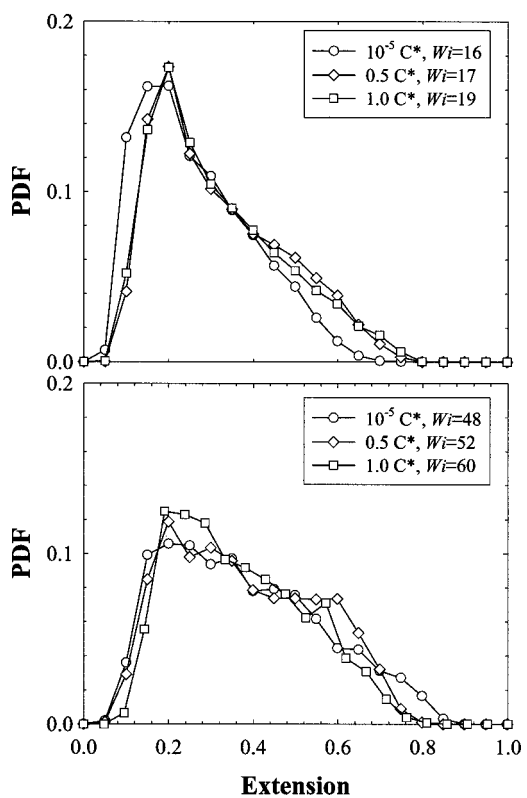


FIG. 9. Probability distribution function of molecular extension at $Wi = 16-19$ and $Wi = 48-60$ for 10^{-5} , 0.5 , and $1.0C^*$ DNA solutions. The molecular extension has been normalized by its contour length.

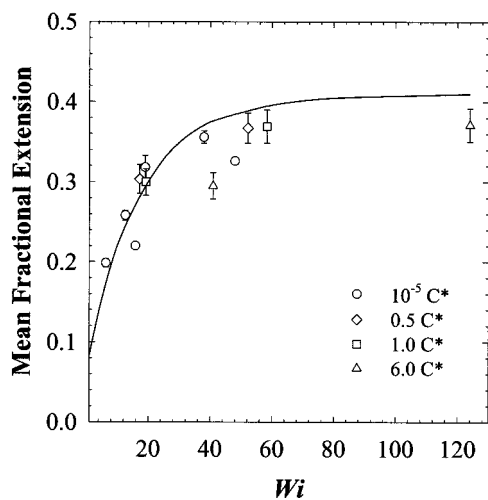


FIG. 10. Steady average molecular extension normalized by the contour length for 10^{-5} , 0.5 , 1.0 , and $6.0C^*$ DNA solutions. No significant concentration effect is observed and all the chain extensions for these solutions asymptote to a value of 0.4 .

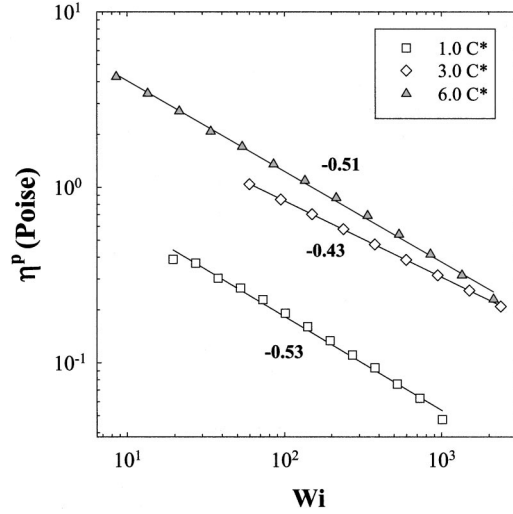


FIG. 11. Polymer shear viscosity (η^{polymer}) of 1, 3, and $6C^*$ DNA solutions. The Wi is calculated based on the longest relaxation time of each solution. All solutions show shear thinning in the range of $10 < Wi < 2000$ with slopes varying from $Wi^{-0.53}$ to $Wi^{-0.43}$.

This derivation was based on calculating the steady average chain conformation thickness (δ_2) of a Kramers' chain in the gradient direction as a function of Wi [Hur *et al.* (2000)] and using the Giesekus stress formula to calculate the polymer shear viscosity [Bird *et al.* (1987)].

The η_{polymer}^s from experiment is shown to scale as

$$\eta_{\text{polymer}}^s \sim Wi^{-0.53} \quad \text{for } 1C^* \text{ solution,} \quad (5)$$

$$\sim Wi^{-0.43} \quad \text{for } 3C^* \text{ solution,} \quad (6)$$

$$\sim Wi^{-0.51} \quad \text{for } 6C^* \text{ solution,} \quad (7)$$

and is in good agreement with the prediction in Eq. (4). This suggests that the shear-thinning exponent of DNA solutions at concentrations up to $6C^*$ can be well predicted by Kramers' chain simulations as long as sufficient internal modes are included [Hur *et al.* (2000)]. This observation that molecules in semidilute DNA solutions behave like a single DNA molecule in a more viscous effective medium is consistent with our findings in Sec. II A 6, where we found perfect overlap of the PSDs as well as similar steady PDFs of molecular extension in solutions at two different DNA concentrations (10^{-5} and $6C^*$) when compared at the same or comparable values of Wi .

2. Transient shear rheology

In this section we consider the transient rheology of DNA solutions with varying DNA concentrations. To compare to the single-molecule microscopy experiments discussed in Sec. II A, we have employed the same 0.5, 1.0, and $6.0C^*$ DNA solutions as used in these experiments, however, we now repeat measurements of the transient shear viscosity (η^+). All measurements were repeated eight times with four different samples for each concentration. The solvent viscosity of each sample was also measured to separate the polymer viscosity (η_{polymer}^+) from the total viscosity (η_{total}^+) for comparison with the

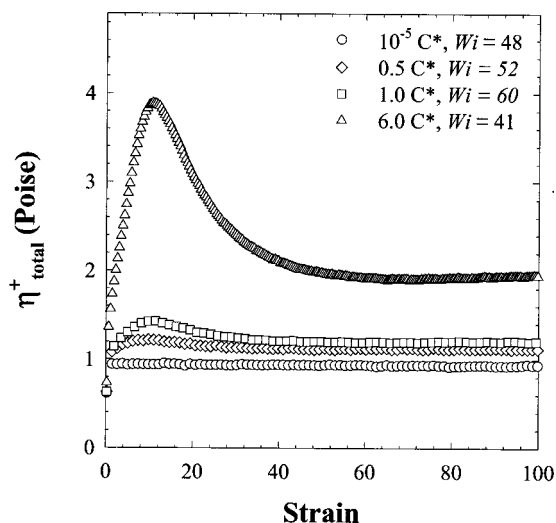


FIG. 12. Total shear viscosity (η_{total}^+) of 10^{-5} , 0.5, 1.0, and $6.0C^*$ DNA solutions at $Wi = 41-60$. In all cases, a pronounced overshoot in η_{total}^+ is observed approximately at strain ($\dot{\gamma}t$) = 10.

data obtained from Brownian dynamics simulations in Sec. III B. The experimental data at lower values of Wi (17–41) reported previously showed an overshoot in shear viscosity [Babcock *et al.* (2000)], and for comparison in this article we present our findings at higher values of Wi .

In Fig. 12, we see an overshoot in η_{total}^+ for the three DNA solutions (0.5, 1.0, and $6.0C^*$) at $Wi = 41-60$. Note that the overshoot occurs at approximately strain ($\dot{\gamma}t$) = 10 for all DNA solutions. Interestingly, this overshoot in η_{total}^+ precedes that in molecular extension (as seen in Sec. II A 5) and is also more pronounced. To further study the overshoot we have examined the transient response of the $1.0C^*$ DNA solution at two values of Wi , 19 and 60. Again, we see a distinctive overshoot in η_{total}^+ and the overshoot seems to occur at strain ($\dot{\gamma}t$) = 10 in Fig. 13 in both cases.

To briefly summarize, we have observed two interesting phenomena from measuring the η_{total}^+ of nondilute DNA solutions. First, a pronounced overshoot in η_{total}^+ is seen to precede that in molecular extension. Second, the strain ($\dot{\gamma}t$) at which such an overshoot is observed is shown to be independent of DNA concentration up to $6C^*$, and apparently independent of Wi as well (as long as we are above the $Wi_c \sim 20$, at which an overshoot is observed).

III. SIMULATION

In Secs. II A and II B we have combined single-molecule microscopy experiments and rheological measurements to investigate the microscopic states and the corresponding macroscopic rheological responses of DNA solutions. It is of great interest to thoroughly understand the experimental findings and gain insight into the nature of the observed transient behavior. To that end, we have used Brownian dynamics simulation to compare our experimental measurements and, furthermore, to establish a clear understanding of the physical basis for our observations.

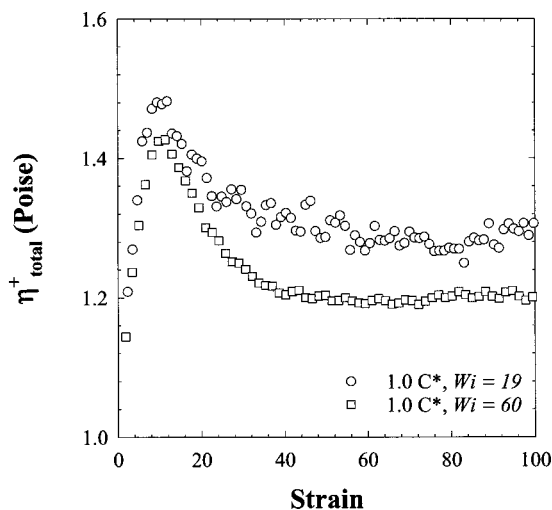


FIG. 13. Total shear viscosity (η_{total}^+) of a $1.0C^*$ DNA solution at $Wi = 19$ and 60 . In both cases, an overshoot in η_{total}^+ is observed again approximately at strain ($\dot{\gamma}t$) = 10 .

A. Methods and models

To understand the dynamics of DNA molecules we have used two models, Kramers' freely jointed bead-rod chains and the worm-like bead-spring chains which were shown to capture the dynamics of isolated single DNA molecules in steady shear flow in our previous work [Hur *et al.* (2000)]. We refer the readers to our previous publication for a more-detailed description of these two models [Hur *et al.* (2000)]. In Kramers' bead-rod chains, a polymer molecule is discretized as a series of beads connected by rigid rods of constant length a (equivalent to the Kuhn length, b_K) and the beads are the centers experiencing the hydrodynamic drag and the Brownian forces. By varying the number of beads, the flexibility of a chain can be varied from a rigid rod ($N = 2$) to an infinitely flexible chain ($N \rightarrow \infty$). In this study we have used 150 bead-rod chains to match the flexibility of the λ -DNA molecules used in the experiments [Hur *et al.* (2000)]. Another widely used mechanical model for the elasticity of a DNA molecule is based on the "worm-like chain" which is equivalent to a long rod with uniform bending stiffness [Bustamante *et al.* (1994)]. To compare to the transient dynamics of Kramer's chain, we use 15-spring worm-like chains in the start-up of shear flow simulations only.

For Kramer's chain, we use the iterative constraint algorithm by Liu [Liu (1989a, 1989b)] to maintain the rod lengths within a given tolerance (typically, $< 10^{-2}a$) and the noise filtering technique by Doyle and Shaqfeh and Grassia and Hinch [Grassia and Hinch (1996); Doyle and Shaqfeh (1998)] for stress calculation. The details of the simulation technique as well as dimensional scalings are discussed elsewhere [Hur *et al.* (2000); Liu (1989a, 1989b); Doyle and Shaqfeh (1998)]. In the Kramer's chain simulations, we nondimensionalize the physical quantities as follows. We scale the length with the interbead distance ($=$ bead diameter or, equivalently, the Kuhn length) a , forces with $k_B T/a$ and time with $\zeta a^2/k_B T$. A dimensionless parameter that measures the strength of the imposed flow is the Peclet number, $Pe = \dot{\gamma} \zeta a^2/k_B T$, which is the ratio of the bead diffusion time scale to the characteristic flow time scale. A more indicative measure of the chain relaxation time scale relative to the characteristic flow scale is the Weissenberg number defined as $Wi = \lambda(N)Pe$, where $\lambda(N)$ is the dimensionless longest relaxation

time of a chain with N beads. The stress and viscosity is then made dimensionless with $n_p k_B T$ and $n_p k_B T \lambda$, respectively, where n_p is the number density. For the worm-like chain simulations, we have developed a second-order full-implicit numerical scheme to calculate the chain trajectories at each time step. This numerical scheme is a generalization of the second-order semi-implicit predictor–corrector scheme as proposed by Öttinger [Öttinger (1995)]. We briefly note that the new algorithm has several advantages over our previous Euler scheme [Hur *et al.* (2000)] in that it is second-order accurate and that it provides better numerical stability, and thus is more efficient. However, the final results presented in this paper obtained by applying either of these algorithms for transient shear flows are identical.

To start any simulation the initial positions of successive beads in the chain are chosen from random vectors distributed over the surface of a unit sphere and these were allowed to thermally equilibrate for a period of 10^7 time steps. After the flow was imposed, the trajectory as well as the stress evolution of the chain was recorded. For all transient shear simulations an ensemble of 60–800 chains were used for Kramer’s chain simulations and 1500–2000 chains for the worm-like chain simulations. For steady shear simulations we only use Kramers’ chains and each chain was allowed to experience a strain of 100–200 to ensure that the chain reached its steady state. After this start-up period, all the steady simulations were then run to a shear strain equal to the experimental shear strain at each value of Wi . The steady molecular extension, i.e., the maximum molecular extension in the flow direction projected in the flow-vorticity plane, was then averaged over the total steady-state sampling time after the start-up period. To obtain average start-up results, the average molecular extension was calculated from the ensemble of chains at every time step. Finally, the transient probability distribution function of the molecular extension is obtained by binning the extension of the ensemble of chains at any given time. To determine the steady-state PDF, molecular extension of a chain was binned at each time step after the start-up period. For convenience, the maximum extension ($N-1$) was divided into 20 bins.

B. Results: Transient shear dynamics

For a direct comparison to the experimental results in Sec. II A 4, we have calculated the average molecular extension of 150 bead Kramers’ chains matching the number of chain ensembles in the experiment (60–100) at $Wi = 6, 13,$ and 38 , as shown in Fig. 14. The simulation qualitatively and nearly quantitatively captures the evolution of average chain deformation; it slightly overpredicts the molecular extension. Again, an overshoot in molecular extension is seen at $\dot{\gamma}t = 20-40$ for $Wi = 38$, as in the experiment. In Fig. 14, the initial rate of increase in molecular extension is shown to be almost independent of Wi in the Wi range we studied. We can compare the measured initial rate to that in the affine limit, i.e., where the molecule moves or deforms like a fluid element. The affine deformation rate v^{aff} in the flow direction for a Hookean dumbbell, for example, is

$$v^{\text{aff}} = \dot{\gamma} \langle |R_2| \rangle, \quad (8)$$

or equivalently,

$$R_1 = R_{1,0} + \langle |R_2| \rangle \dot{\gamma} t. \quad (9)$$

In Eqs. (8) and (9), $\langle |R_2| \rangle$ is the average absolute equilibrium length of a Hookean dumbbell in the gradient direction and R_1 is the chain extension in the flow direction where the superscript “0” denotes an initial value. Thus, the initial chain deformation in

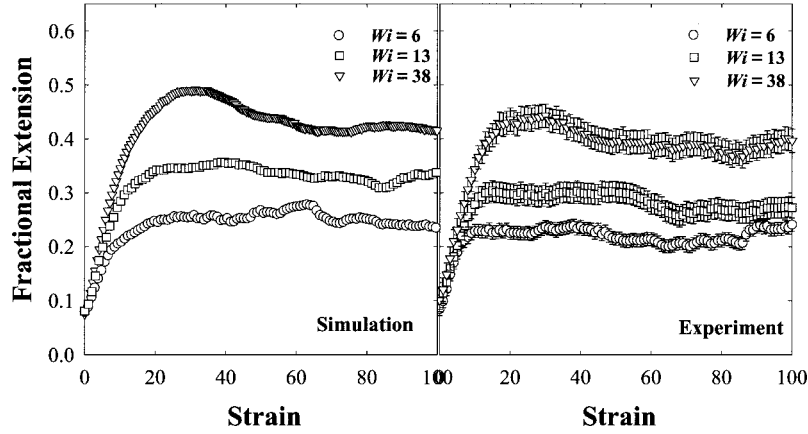


FIG. 14. Average molecular extension of 150 bead chains at $Wi = 6, 13,$ and 38 . The extension has been normalized by its maximum extension. The simulation slightly overpredicts the molecular extension. An overshoot in molecular extension is observed at $Wi = 38$.

the affine limit in the flow direction per strain ($\dot{\gamma}t$) is directly related to the average equilibrium chain extension in the gradient direction. $\langle |R_2| \rangle$ can be calculated near equilibrium as

$$\langle |R_2| \rangle = \int_{-\infty}^{\infty} |R_2| \psi(R_2) dR_2, \quad (10)$$

$$= \frac{1}{R_g} \sqrt{\frac{3}{2\pi}} \int_0^{\infty} R_2 e^{-(3/8R_g^2)R_2^2} dR_2, \quad (11)$$

$$= \sqrt{\frac{8}{3\pi}} R_g. \quad (12)$$

In Eq. (10), $\psi(R_2)$ is the probability distribution function of R_2 [Bird *et al.* (1987)] and R_g is the radius of gyration. The analytic value of $\sqrt{(8/3\pi)}R_g$ has been compared to the values from Brownian dynamics simulation of Hookean dumbbells, and only at $Wi = 1000$ does the chain deformation reach 99% of its affine rate. This value of Wi at which affine motion is achieved is much higher than that of uniaxial extensional flow where affine deformation is observed at Wi as low as 48 [Smith and Chu (1998)]. This clearly demonstrates that uniaxial extensional flow is more effective in unraveling an initially coiled chain than shear flow. We can extend the derivation in Eq. (10) for a long Gaussian bead-spring chain ($N \gg 1$), and the analytic affine deformation rate is given by

$$\langle |R_2| \rangle = \frac{2}{\sqrt{\pi}} R_g. \quad (13)$$

The initial chain deformation rates of dilute and semidilute DNA solutions have been analyzed and are summarized in Table I. We can see that the initial deformation rates from our experiment have only reached 60%–70% of the affine limit value, suggesting that at $Wi = 38$ –60 a DNA molecule does not deform nearly as fast as a fluid element.

TABLE I. Initial deformation rates of 10^{-5} , $0.5C^*$, and $1.0C^*$ DNA solutions are compared to that in the affine limit at $Wi = 38-60$.

DNA concentration (C^*)	Wi	% affine
10^{-5}	38	67
10^{-5}	48	59
0.5	52	57
1.0	60	58

The initial ‘‘subaffine’’ deformation is then followed by an overshoot in molecular extension above a critical Wi at values of strains $\dot{\gamma}t = 20-40$. This overshoot is not seen in any linear force models such as the Rouse or Zimm model [Bird *et al.* (1987)] and we find that it is related to the nonaffine motion of the chain. As seen in Fig. 15, at low values of Wi the chain thickness in the gradient direction ($\sqrt{\langle R_2^2 \rangle}$) is found to remain nearly constant on flow inception, whereas at high Wi (above a critical Wi where an overshoot in molecular extension is observed) the chain thickness in the gradient direction starts to slowly decrease after $\dot{\gamma}t = 9-10$ to its steady value. We find the overshoot in shear viscosity occurs during this initial alignment, as shown in Fig. 16. The initial growth of shear viscosity (η_{polymer}^+) is due to the chain expansion in the flow direction from a coiled state while maintaining constant chain dimension in the gradient direction. Physically, the pronounced overshoot (or, equivalently, a maximum in shear viscosity) at $\dot{\gamma}t \approx 10$ corresponds to the point where the chain starts to ‘‘feel’’ its finite extensibility and the nonlinear entropic force [Bird *et al.* (1987); Bustamante *et al.* (1994)]. The shear flow then begins to rotate the chain about the vorticity axis toward the stagnation line through the chain center of mass until it enters the Graetz–Levecque layer [i.e., the region where diffusion of chain segments balances convection, see Hur *et al.* (2000)]. The chain dimension or thickness in the gradient direction starts to decrease at this point. As the extended chain enters the Graetz–Levecque layer where smaller hydrodynamic forces (or smaller relative velocity between chain segments) are exerted, the chain cannot maintain its extension and this leads to an ‘‘average’’ retraction in molecular extension.

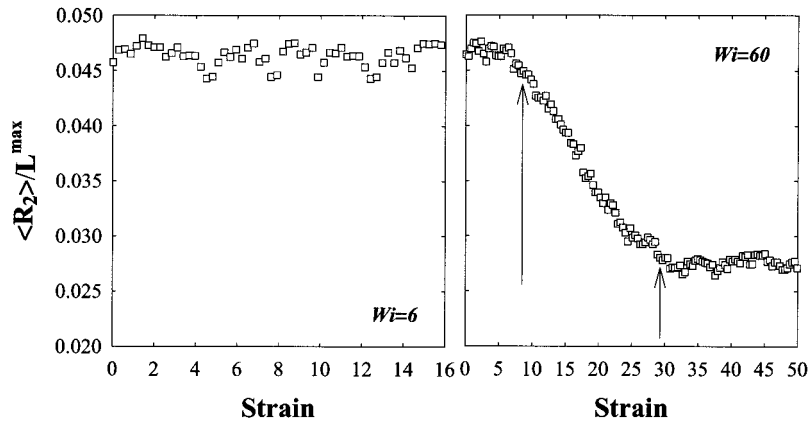


FIG. 15. Normalized chain thickness ($\sqrt{\langle R_2^2 \rangle}/L$) in the gradient direction. At $Wi = 6$, $\sqrt{\langle R_2^2 \rangle}/L$ remains constant during the start-up. The noises are due to larger Brownian fluctuations at low Wi . At $Wi = 60$, $\sqrt{\langle R_2^2 \rangle}/L$ starts to decrease at $\dot{\gamma}t = 9-10$.

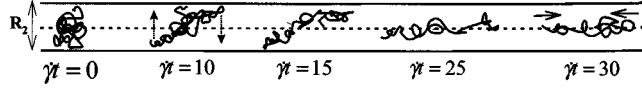


FIG. 16. Schematic of chain deformation in the start-up of shear flow.

This argument is further verified in Fig. 15 where we see the chain thickness starts to decrease at the strain where an overshoot in shear viscosity is observed and the thickness reaches its steady state at the strain where a maximum in extension is observed at $Wi = 20$. In comparison, the much less-pronounced overshoot in molecular extension for all DNA solutions in Fig. 5 can be understood from the PDF at $\dot{\gamma}t = 30$ and 100 from simulation, as in Fig. 17 where the two distributions of chain extension are not significantly different. Even though at $\dot{\gamma}t = 30$ the chain configuration is shifted towards a more highly extended state, the distribution is almost uniform with equal probability of all chain extension except for very coiled or highly extended states, at approximately ~ 0.1 , thus the average chain extension does not demonstrate a very pronounced overshoot. In Fig. 18, we make a direct comparison between the experimental and simulation data of the shear viscosity and molecular extension at $Wi = 20$ and we see good agreement, which is also seen at $Wi = 60$ [Babcock *et al.* (2000)] for the 150 bead Kramers' chains. The worm-like chain qualitatively captures the transient shear viscosity but predicts an overshoot in viscosity at a slightly higher strain than both the Kramers' chain and the experimental data, as shown in Fig. 19. On the other hand, the average molecular extension is well predicted by both models in comparison to the experimental data (see Fig. 20).

Based on the observations above, we can predict the strain at which the shear viscosity undergoes an overshoot in the “affine” limit. We assume the chain must reach some length L^{aff} before it starts to “feel” its maximum extensibility or the nonlinear entropic force, viz.

$$\sqrt{\langle |R_1| \rangle^2 + \langle R_2^2 \rangle + \langle R_3^2 \rangle} \approx L^{\text{aff}}. \quad (14)$$

In Eq. (14), 1, 2, and 3 denote the flow direction, the gradient direction, and the vorticity direction, respectively. We have found from our experiments and simulations that L^{aff} is around 30%–40% of the chain contour length (L). We further assume that $\langle R_2^2 \rangle$ and $\langle R_3^2 \rangle$ are constant in the initial deformation stage as follows:

$$\langle |R_1| \rangle = \frac{2}{\sqrt{\pi}} R_g (1 + \dot{\gamma}t), \quad (15)$$

$$\langle R_2^2 \rangle + \langle R_3^2 \rangle \approx 4R_g^2, \quad (16)$$

$$L^{\text{aff}} \approx \frac{3}{10} \sqrt{6NR_g}. \quad (17)$$

In Eq. (15), N is the number of rods or Kuhn steps and we have set $L^{\text{aff}} = 0.3L$ based on our data. The strain ($\dot{\gamma}t^{\text{crit}}$) at which the chain starts to experience a nonlinear increase in its entropic restoring force is then

$$\dot{\gamma}t_{\text{affine}}^{\text{crit}} \approx \frac{3}{20} \sqrt{6\pi N} - 1, \quad N \gg 1. \quad (18)$$

This result shows that the critical strain, $\dot{\gamma}t^{\text{crit}}$, depends on the molecular weight and is independent of Wi (for $Wi > Wi^{\text{crit}}$) in the affine limit. λ -DNA has about 150 Kuhn

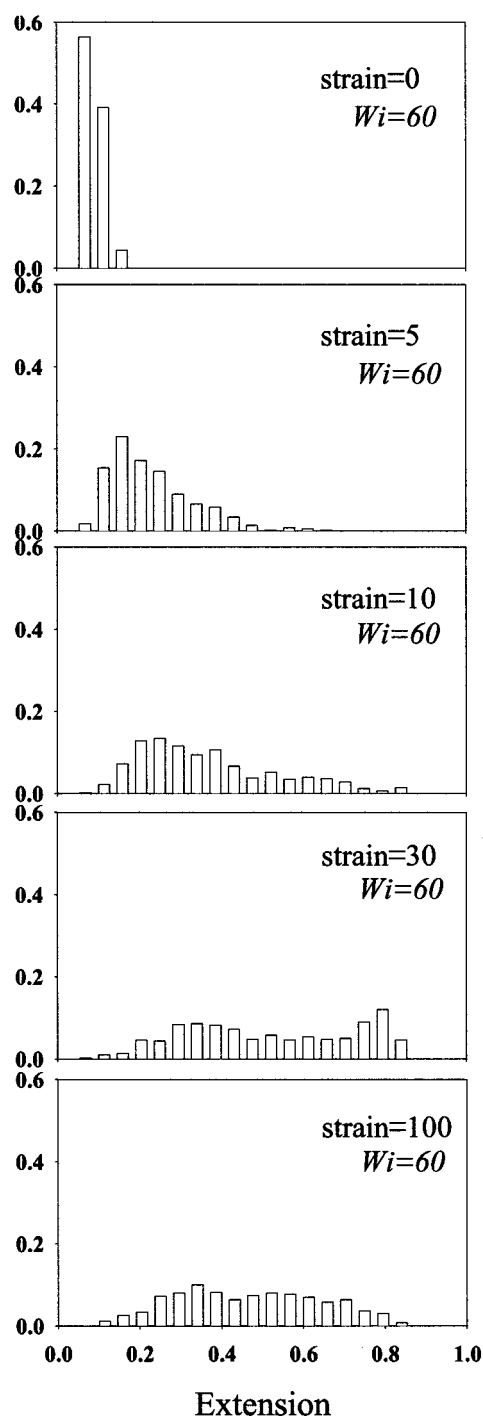


FIG. 17. Transient PDF of molecular extension of 150 bead chains at $Wi = 60$. A population of highly extended chains starts to appear at $\gamma t = 30$ but is almost uniform.

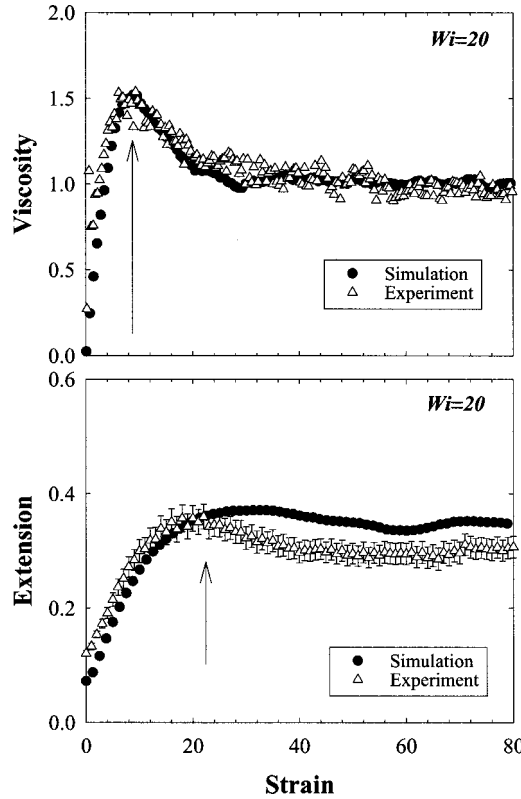


FIG. 18. Comparison between simulation and experiment. The normalized average molecular extension and shear viscosity of an ensemble of 400 chains ($N = 150$) at $Wi = 20$ are in good agreement with experiment. The overshoot in shear viscosity is more pronounced and it precedes that in molecular extension. The quantitative difference in molecular extension between simulation and experiment is smaller than the noise in the experiment due to a smaller ensemble size.

steps [Bustamante *et al.* (1994)] and this gives $\dot{\gamma}t^{\text{crit}} \approx 7$, which is close to that shown in Figs. 12 and 13. The slight discrepancy between this value and the value of $\dot{\gamma}t^{\text{crit}} = 10$ –11 from experiment can be reduced by taking into account the fact that at $Wi = 60$ the deformation is only subaffine (see Table I). The analytic expression for $\dot{\gamma}t^{\text{crit}}$ (subaffine) is

$$\dot{\gamma}t_{\text{subaffine}}^{\text{crit}} \approx \frac{1}{\epsilon(Wi)} \frac{3}{20} \sqrt{6\pi N} - 1, \quad N \gg 1. \quad (19)$$

In Eq. (19), $\epsilon(Wi)$ is a parameter characterizing the degree to which the initial stretch rate is affine. It takes a value of 1 in the affine limit ($Wi \rightarrow \infty$) and is shown to be 0.6–0.7 at $Wi = 60$ from experiment. Using again $N = 150$, $\dot{\gamma}t_{\text{subaffine}}^{\text{crit}}$ at $Wi = 60$ is 10–12, in better agreement with the experimental value. Based on this scaling result, we anticipate the overshoot in shear viscosity to occur at lower strain as we increase the flow strength (or Wi) and eventually reach $\dot{\gamma}t_{\text{affine}}^{\text{crit}}$. We have further tested this scaling with varying N ($N = 50, 100, 150, 200$, and 220) in our simulations and confirmed that $\dot{\gamma}t^{\text{crit}} + 1$ scales as \sqrt{N} (see Fig. 21) at $Wi = 60$ and also at $Wi = 300$. For linear force

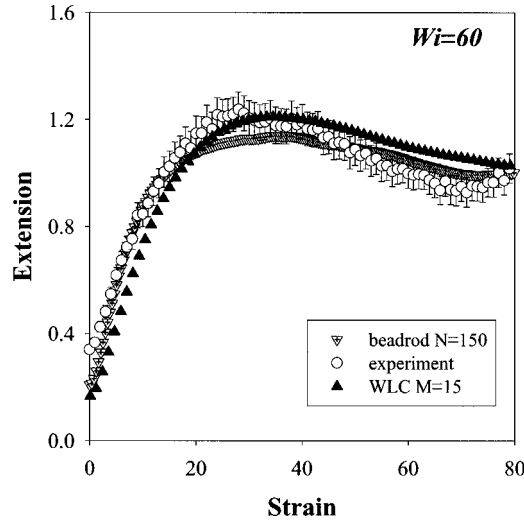


FIG. 19. Normalized shear viscosity of 15-spring worm-like chains and Kramers' chains compared to the experimental data at $Wi = 60$.

models which correspond to $N \rightarrow \infty$, according to Eq. (19) the critical strain is infinite, and thus no overshoot is predicted.

We have also calculated the dependence of the extent of the overshoot in shear viscosity relative its steady-state value for $Wi > Wi^{\text{crit}}$ on chain size (N) and Wi . In the simulation, we used $N = 50, 100, \text{ and } 150$ and the range of Wi is $60\text{--}300$. Combining the findings in Figs. 22 and 23, we obtain

$$\frac{\eta_{\text{polymer}}^{+, \text{max}}}{\eta_{\text{polymer}}^s} \sim \frac{Wi^{0.4-0.45}}{N^{1/3}}, \quad N \gg 1, \quad \text{and } Wi \gg Wi^{\text{crit}}. \quad (20)$$

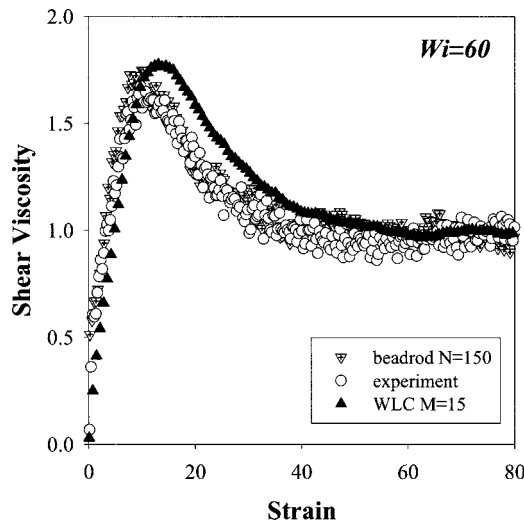


FIG. 20. Normalized average molecular extension of 15-spring worm-like chains and Kramers' chains compared to the experimental data at $Wi = 60$.

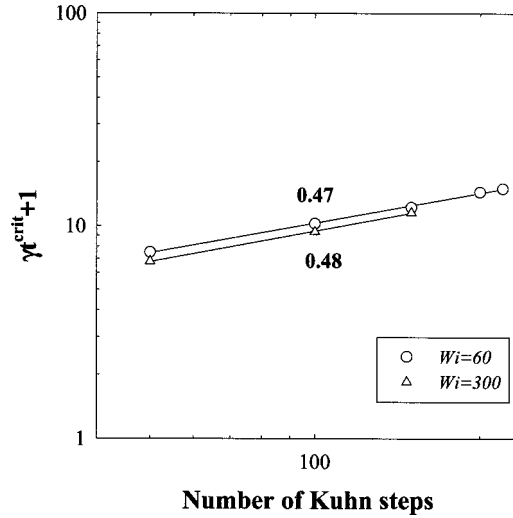


FIG. 21. Dependence of the critical strain at which an overshoot in shear viscosity occurs on the number of internal modes.

The Wi scaling can be predicted from our previous finding [cf. Hur *et al.* (2000)] as follows [see Sec. II B 1, Eq. (4)]:

$$\frac{\eta_{\text{polymer}}^{+, \text{max}}}{\eta_{\text{polymer}}^s} \sim \frac{1}{Wi^{-1/2}} \sim Wi^{1/2}, \quad Wi \gg Wi^{\text{crit}}, \quad (21)$$

where we assume that the polymer shear viscosity at the point of overshoot ($\eta_{\text{polymer}}^{+, \text{max}}$) saturates in the high Wi limit ($Wi \gg Wi^{\text{crit}}$), and thus is independent of Wi . The predicted scaling of $Wi^{1/2}$ is close to that found in the simulation as in Eq. (20). We note that

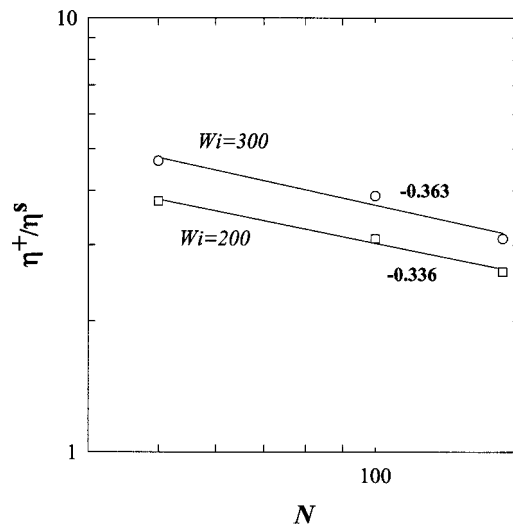


FIG. 22. Dependence of $\eta_{\text{polymer}}^{+, \text{max}} / \eta_{\text{polymer}}^s$ on chain size (N) at $Wi = 200$ and 300 . The slope is close to $-\frac{1}{3}$.

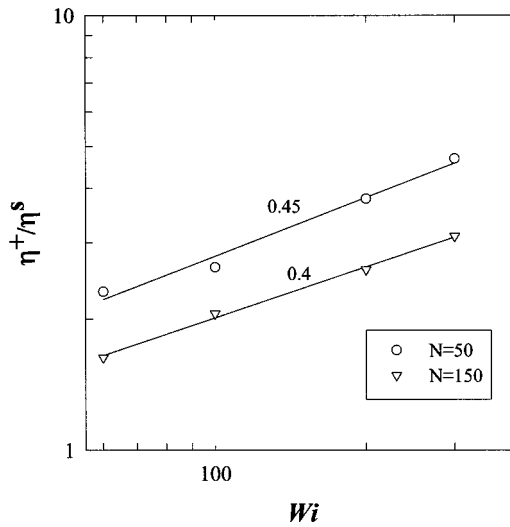


FIG. 23. Dependence of $\eta_{\text{polymer}}^{+, \text{max}} / \eta_{\text{polymer}}^s$ on Wi for $N = 50, 100,$ and 150 . The slope is 0.45 for $N = 50$ and close to 0.4 for $N = 150$.

in the Wi range of $60\text{--}300$, $\eta_{\text{polymer}}^{+, \text{max}}$ was found to have a weak Wi dependence of $Wi^{-\beta}$; $0.05 < \beta < 0.1$, which explains the slight discrepancy between the predicted scaling of $Wi^{1/2}$ and the calculated scaling of $Wi^{2/5}$. From Eq. (20) one anticipates the magnitude of the overshoot in shear viscosity to increase with Wi (like $Wi^{0.4}$), and decrease with molecular weight (like $Mw^{-1/3}$).

Interestingly, as shown in Fig. 24, we found that the ratio of $\eta_{\text{polymer}}^{+, \text{max}} / \eta_{\text{polymer}}^s$ is related to the extent of thinning of chain dimension in the gradient direction [$(\sqrt{\langle \delta_{2, \text{max}}^2 \rangle} / \sqrt{\langle \delta_{2, s}^2 \rangle})$], where δ_2 is defined as

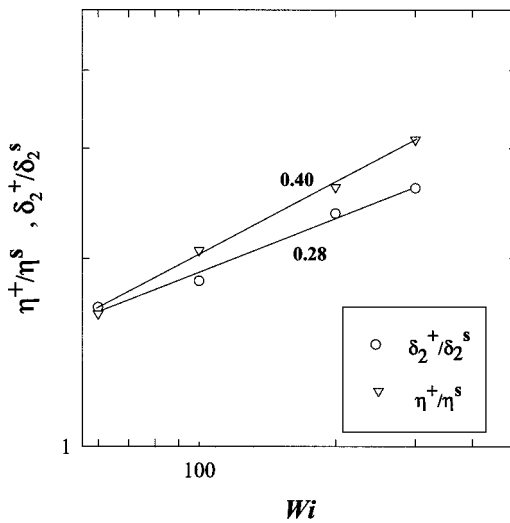


FIG. 24. Comparison of $\eta_{\text{polymer}}^{+, \text{max}} / \eta_{\text{polymer}}^s$ and $\sqrt{\langle \delta_{2, \text{max}}^2 \rangle} / \sqrt{\langle \delta_{2, s}^2 \rangle}$ at different values of Wi from simulation for 150 bead-rod chains.

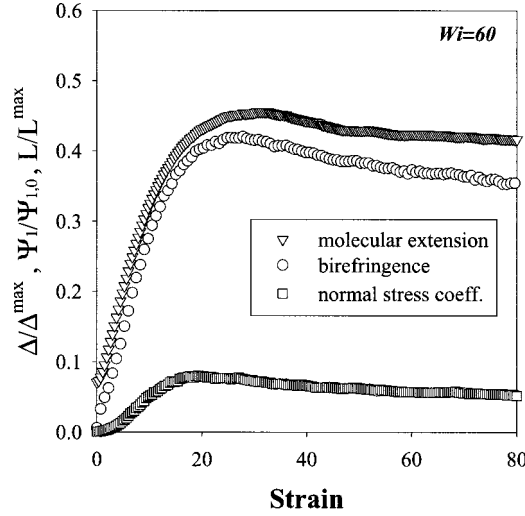


FIG. 25. Transient first normal stress and birefringence calculated from 400 chains of 150 beads at $Wi = 60$. For comparison, the evolution of molecular extension is plotted.

$$\langle \delta_2^2 \rangle = \left\langle \frac{1}{N} \sum_{\nu=1}^N R_2^\nu R_2^\nu \right\rangle, \quad (22)$$

and R_2^ν is the position vector of bead ν relative to the center of mass of the chain in the gradient direction. This ratio has a different Wi dependence, and is close to $Wi^{1/4}$, which can be predicted from our previous work [Hur *et al.* (2000)]:

$$\frac{\sqrt{\langle \delta_{2,\max}^2 \rangle}}{\sqrt{\langle \delta_{2,s}^2 \rangle}} \sim \frac{1}{Wi^{-1/4}} \sim Wi^{1/4}. \quad (23)$$

In Eq. (23), $\langle \delta_{2,\max}^2 \rangle$ is simply the equilibrium chain dimension in the gradient direction, and thus depends only on N .

Finally, we have extended our analysis to examine other transient rheological properties and their relationship to the changes in the molecular state. In general, viscoelastic stresses are produced by distortions of the polymer configuration. For Gaussian chains the steady-state stress tensor is directly proportional to the second moment of the chain configuration distribution [Bird *et al.* (1987)]. Mechanical stresses can, therefore, be interpreted in terms of anisotropies in molecular orientations [Larson (1988)]. Two widely measured properties to characterize such anisotropies are the first normal stress difference ($N_1 = \tau_{11} - \tau_{22}$) and birefringence ($\Delta' = n_{11} - n_{22}$).

We have also calculated the first normal stress coefficient ($\psi_1 = N_1 / Pe^2$) and birefringence (Δ') of an ensemble of 150 bead chains at $Wi = 60$ in our simulation. In Fig. 25 one can see similar characteristics in both quantities compared to that in molecular extension in the flow direction, i.e., both the first normal stress and birefringence do not exhibit as pronounced an overshoot as that characterizing the shear viscosity and both properties overshoot at a later strain ($\dot{\gamma}t^{\text{crit}} = 20-40$) than the shear viscosity which overshoots at $\dot{\gamma}t^{\text{crit}} \approx 10$.

C. Results: Chain overlap and semidilute scaling

The main findings in Secs. II B 1 and II A 6 suggest that the steady dynamics of DNA solutions up to $6C^*$ can be essentially explained by the dynamics of an isolated DNA chain by properly adjusting the chain diffusion time scale. In our earlier work [Hur *et al.* (2000)], we have demonstrated that Brownian dynamics simulations of a single Kramers' chain matching the molecular parameters of a λ -DNA molecule is capable of explaining the steady dynamics of these DNA solutions [Smith *et al.* (1999)]. Thus, we refer the readers to our previous work for more-detailed discussions. In this section, we calculate the spacing between the *configuration space* of the individual chains in the semidilute regime. The main idea is to treat the chains undergoing tumbling, stretching in a cigar-shaped Graetz–Leveque layer of a thickness δ_2 at steady state, as a homogeneous dispersion of randomly positioned, aligned semidilute rigid rods [Batchelor (1971); Shaqfeh and Fredrickson (1990)] of a diameter δ_2 , where the interparticle spacing d is known to scale as

$$d = \frac{1}{(\pi n_p L)^{1/2}}, \quad (24)$$

where n_p and L denote the number density and the length of the rods, respectively. By semidilute we mean $d/L \ll 1$. Using the parameters from the experiment, we calculate d/L for $6C^*$ DNA solutions at $Wi = 60$, where L in our case is half the contour length of a DNA molecule, namely, $L = 8.15 \mu\text{m}$,

$$\frac{d}{L} = \frac{1}{[\pi \times 4.33 \times 10^{12} \text{ ml}^{-1} (8.15 \mu\text{m})^3]^{1/2}} = 0.0117. \quad (25)$$

This confirms that at $6C^*$, the DNA molecules are indeed in the semidilute regime. One immediate consequence of this is that inter- and intrachain hydrodynamic interactions are screened in this regime and these have been neglected in the simulations [Mackaplow and Shaqfeh (1998); Doi and Edwards (1986)]. From Eq. (25) the average interchain spacing d is $0.095 \mu\text{m}$. It is remarkable that even though d is substantially smaller than the Graetz–Leveque layer thickness ($\delta_2 = 0.56 \mu\text{m}$) at $Wi = 60$ calculated from simulation that no qualitative or quantitative difference is demonstrated in the PSD. Note that d is still much larger than the molecular thickness (4 nm) [Pecora (1991)]. This calculation, together with our experimental findings presented in the previous sections, suggest that the nonequilibrium dynamics of semidilute DNA solutions is not altered in character despite an overlap of individual chains in configuration space.

IV. CONCLUSION

We have combined single-molecule fluorescence microscopy, bulk rheological measurement, and Brownian dynamics simulation to investigate the dynamics of dilute and semidilute DNA solutions in both start-up and steady shear flow. Our data show that there is an overshoot in molecular extension for all DNA solutions at high flow strength. This overshoot is shown to occur after a pronounced overshoot in polymer shear viscosity for the same DNA solution at the same Wi . Simulations suggest that the overshoot in shear viscosity at high Wi is created by highly extended chains rotating toward the stagnation line and entering the Graetz–Leveque boundary layer to align with the flow. A simple scaling is given to predict the critical strain ($\dot{\gamma}t$) at which such an overshoot occurs. Once the chain starts to align and falls within the Graetz–Leveque layer, it cannot maintain its extended state due to smaller relative chain velocities near the stag-

nation line, and an average retraction in molecular extension follows. Both overshoots are not due to polymer–polymer interactions. We have further shown that by studying the transient chain deformation in the flow direction one can qualitatively predict the evolution of birefringence and the first normal stress difference. The analysis of both experimental and simulation data in steady shear flow suggests that polymer concentration has no effect on the dynamics other than increasing the viscosity of the medium. Thus, by scaling with the longest polymer relaxation time, one can understand the dynamics of semidilute solutions by an effective mean-field approach. In future work, it would be of great use and of importance to directly measure the chain dimension in the gradient direction since many rheological properties in steady shear flow are directed related to this quantity. Also, multichain simulations might be useful to further broaden our understanding of the dynamics in the semidilute regime.

ACKNOWLEDGMENTS

This work was supported in part by U.S. AFOSR, the NSF, the Human Frontiers Foundation, and by an endowment established by Theodore and Frances Geballe. Two of the authors (J.S.H. and E.S.G.S.) were funded by NSF under CPIMA Cooperative Agreement No. DMR-9808677. One of the authors (H.P.B.) was supported in part by a NIH biophysics training grant and in part by CPIMA. One of the authors (D.E.S.) received support from a NSF fellowship in Mathematics and Molecular Biology.

References

- Babcock, H. P., D. E. Smith, J. S. Hur, E. S. G. Shaqfeh, and S. Chu, “Relating the microscopic and macroscopic response of a polymeric fluid in a shearing flow,” *Phys. Rev. Lett.* **85**, 2018–2021 (2000).
- Batchelor, G. K., “The stress generated in a nondilute suspension of elongated particles by pure straining motion,” *J. Fluid Mech.* **46**, 813–829 (1971).
- Bird, R. B., C. F. Curtiss, R. C. Armstrong, and O. Hassager, *Dynamics of Polymeric Liquids: Volume 2, Kinetic Theory* (Wiley, New York, 1987).
- Bustamante, C., J. F. Marko, E. D. Siggia, and S. Smith, “Entropic elasticity of lambda-phage DNA,” *Science* **265**, 1599–1600 (1994).
- Carl, W., “Finitely extensible bead spring chains in time-dependent shear flows,” *Rheol. Acta* **36**, 2227–2234 (1997).
- Chow, A. W., G. G. Fuller, D. G. Wallace, and J. A. Madri, “Rheo-optical response of rodlike, shortened collagen protein to transient shear flow,” *Macromolecules* **18**, 805–810 (1985).
- Cifre, J. G. H. and J. G. de la Torre, “Steady-state behavior of dilute polymers in elongational flow: Dependence of the critical elongational rate on chain length, hydrodynamic interaction, and excluded volume,” *J. Rheol.* **43**, 339–358 (1999).
- de Gennes, P. G., *Scaling Concepts in Polymer Physics* (Cornell University Press, Ithaca, NY, 1979).
- de Gennes, P. G., “Polymer physics: Molecular individualism,” *Science* **276**, 1999 (1997).
- Doi, M. and S. F. Edwards, *The Theory of Polymer Dynamics* (Oxford Science, Oxford, U.K., 1986).
- Doyle, P. S., E. S. G. Shaqfeh, and A. P. Gast, “Dynamic simulation of freely draining, flexible polymers in steady linear flows,” *J. Fluid Mech.* **334**, 251–291 (1997).
- Doyle, P. S. and E. S. G. Shaqfeh, “Dynamic simulation of freely draining flexible bead-rod chains: Start-up of extensional and shear flow,” *J. Non-Newtonian Fluid Mech.* **76**, 43–78 (1998).
- Doyle, P. S., B. Ladoux, and J. L. Viovy, “Dynamics of a tethered polymer in shear flow,” *Phys. Rev. Lett.* **84**, 4769–4772 (2000).
- Dua, A. and B. J. Cherayil, “Chain dynamics in shear flow,” *J. Chem. Phys.* **112**, 8707–8714 (2000).
- Evans, A. R., E. S. G. Shaqfeh, and P. L. Frattini, “Observations of polymer conformation during flow-through a fixed-fiber bed,” *J. Fluid Mech.* **281**, 319–356 (1994).
- Grassia, P. S. and E. J. Hinch, “Computer simulations of polymer chain relaxation via Brownian motion,” *J. Fluid Mech.* **308**, 255–288 (1996).
- Huppeler, J. P., I. F. Macdonald, E. Ashare, T. W. Spriggs, R. B. Bird, and L. A. Holmes, *Trans. Soc. Rheol.* **11**, 181–191 (1967).

- Hur, J. S., E. S. G. Shaqfeh, and R. G. Larson, "Brownian dynamics simulations of single DNA molecules in shear flow," *J. Rheol.* **44**, 713–742 (2000).
- Janeschitz-Kriegl, H., *Polymer Melt Rheology and Flow Birefringence* (Springer, New York, 1983).
- Kume, T., T. Hattori, and T. Hashimoto, "Time evolution of shear-induced structures in semidilute polystyrene solutions," *Macromolecules* **30**, 427–434 (1997).
- Larson, R. G., *Constitutive Equations for Polymer Melts and Solutions* (Butterworths, New York, 1988).
- Larson, R. G., T. T. Perkins, D. E. Smith, and S. Chu, "Hydrodynamics of a DNA molecule in a flow field," *Phys. Rev. E* **55**, 1794–1797 (1997).
- Larson, R. G., H. Hu, D. E. Smith, and S. Chu, "Brownian dynamics simulations of a DNA molecule in an extensional flow field," *J. Rheol.* **43**, 267–304 (1999).
- Lee, E. C., M. J. Solomon, and S. J. Muller, "Molecular orientation and deformation of polymer solutions under shear: A flow light-scattering study," *Macromolecules* **30**, 7313–7321 (1997).
- Li, L. and R. G. Larson, "Comparison of Brownian dynamics simulations with microscopic and light-scattering measurement of polymer deformation under flow," *Macromolecules* **33**, 1411–1415 (2000).
- Link, A. and J. Springer, "Light scattering from dilute polymer solutions in shear flow," *Macromolecules* **26**, 464–471 (1993).
- Liu, T. W., Ph.D. thesis, University of Wisconsin (1989a).
- Liu, T. W., "Flexible polymer chain dynamics and rheological properties in steady flows," *J. Chem. Phys.* **90**, 5826–5842 (1989b).
- Lyulin, A. V., D. B. Adolf, and G. R. Davies, "Brownian dynamics simulations of linear polymers under shear flow," *J. Chem. Phys.* **111**, 758–771 (1999).
- Mackaplow, M. B. and E. S. G. Shaqfeh, "A numerical study of the sedimentation of fiber suspensions," *J. Fluid Mech.* **376**, 149–182 (1998).
- Magda, J. J., C. S. Lee, S. J. Muller, and R. G. Larson, "Rheology, flow instabilities, and shear-induced diffusion in polystyrene solutions," *Macromolecules* **26**, 1696–1706 (1993).
- McLeish, T. C. B., J. Allgaier, D. K. Bick, G. Bishko, P. Biswas, R. Blackwell, B. Blottiere, N. Clarke, B. Gibbs, D. J. Groves, A. Hakiki, R. K. Heenan, J. M. Johnson, R. Kant, D. J. Read, and R. N. Young, "Dynamics of entangled H-polymer: Theory, rheology, and neutron scattering," *Macromolecules* **32**, 6734–6758 (1999).
- Ng, R. C. Y. and L. G. Leal, "Concentration effects on birefringence and flow modification of semidilute polymer solutions in extensional flows," *J. Rheol.* **37**, 443–468 (1993).
- Ottinger, H. C., *Stochastic Processes in Polymeric Liquids* (Springer, Berlin, 1995).
- Pecora, R., "DNA: A model compound for solution studies of macromolecules," *Science* **251**, 893–898 (1991).
- Perkins, T. T., D. E. Smith, and S. Chu, "Direct observation of tube-like motion of a single polymer chain," *Science* **264**, 819–822 (1994).
- Perkins, T. T., D. E. Smith, R. G. Larson, and S. Chu, "Stretching of a single tethered polymer in a uniform flow," *Science* **268**, 83–87 (1995).
- Perkins, T. T., D. E. Smith, and S. Chu, "Single polymer dynamics in an elongational flow," *Science* **276**, 2016–2021 (1997).
- Shaqfeh, E. S. G. and G. Fredrickson, "The hydrodynamic stress in a suspension of rods," *Phys. Fluids A* **2**, 7–24 (1990).
- Smith, D. E. and S. Chu, "Response of flexible polymers to a sudden elongational flow," *Science* **281**, 1335–1340 (1998).
- Smith, D. E., H. P. Babcock, and S. Chu, "Single polymer dynamics in steady shear flow," *Science* **283**, 1724–1727 (1999).
- van den Brule, B. H. A. A., "Brownian dynamics simulation of finitely extensible bead spring chains," *J. Non-Newtonian Fluid Mech.* **47**, 357–378 (1993).